

Phonons in single and few-layer MoS₂ and WS₂

A. Molina-Sánchez* and L. Wirtz

*Institute for Electronics, Microelectronics, and Nanotechnology (IEMN),
CNRS-UMR 8520, Department ISEN, B.P. 60069, 59652 Villeneuve d'Ascq, France*

(Dated: November 27, 2024)

We report *ab-initio* calculations of the phonon dispersion relations of the single-layer and bulk dichalcogenides MoS₂ and WS₂. We explore in detail the behavior of the Raman active modes, A_{1g} and E_{2g}^1 as a function of the number of layers. In agreement with recent Raman spectroscopy measurements [C. Lee et. al., ACS Nano 4, 2695 (2010)] we find that the A_{1g} mode increases in frequency with increasing layer number while the E_{2g}^1 mode decreases. We explain this decrease by an enhancement of the dielectric screening of the long-range Coulomb interaction between the effective charges with growing number of layers. This decrease in the long-range part over-compensates the increase of the short-range interaction due to the weak inter-layer interaction.

PACS numbers: 63.10.+a,63.20.dk,71.15.Mb

I. INTRODUCTION

Recently, the mechanical exfoliation technique, applied to layered materials, has led to the fabrication of new bidimensional systems, i.e., atomically thin layers.¹ Graphene,² a planar sheet of carbon atoms arranged in a hexagonal lattice, is the most famous bidimensional material and exhibits intriguing physical properties not found in its bulk counterpart graphite.^{3,4} However, the absence of a bandgap makes its use in electronic devices (transistors) difficult. Several strategies were proposed to overcome this setback by opening a gap: quantum confinement in nanoribbons,⁵ deposition of a graphene monolayer on boron nitride,⁶ applying an electric field in bilayer graphene,⁷ etc. Nevertheless, the experimental realization of a bandgap larger than 400 meV remains a challenge,⁸ besides of a deterioration of other graphene properties, in particular the high mobility. Therefore, the fabrication of atomically thin sheets of other materials, with a finite bandgap, appears as the natural strategy in the search of materials for a new generation of electronic devices.

In recent experiments, molybdenum disulfide (MoS₂), an indirect semiconductor of bandgap 1.29 eV in its bulk phase, has exhibited a direct bandgap of 1.75 eV in its single-layer phase, together with an enhancement of the luminescence quantum yield in comparison with the MoS₂ bulk.^{9,10} Moreover, Radisavljevic *et. al.*¹¹ have demonstrated suitable properties of a single-layer MoS₂-based transistor, like a room-temperature electron mobility close to that of graphene nanoribbons and a high on/off ratio. Therefore, single-layer MoS₂ has become an appealing material in the area of optoelectronic devices, being an alternative and/or complement to graphene. From other layered compounds such as WS₂, MoS₂, BN, ... monolayers can be produced by (liquid) exfoliation as well.¹² Moreover, MoS₂ and other layered materials are also interesting due to change of certain properties with respect to its bulk counterparts. Finally, their topology facilitates the chemical identification atom-by-atom.¹³

Recent Raman spectroscopy measurements of MoS₂ single and multi-layers have revealed unexpected trends of the vibrational properties when the number of layers changes. Lee *et. al.*¹⁴ reported a decrease in frequency of the optical E_{2g}^1 phonon mode with increasing number of layers. This is consistent with the finding that in bulk MoS₂ the infrared active E_{1u} mode (where neighboring layers are vibrating in-phase) is slightly lower in frequency than the Raman active E_{2g}^1 mode (where neighboring layers are vibrating with a phase shift of π).¹⁵ But both observations contradict the naive expectation that the weak inter-layer forces should increase the effective restoring forces acting on atoms. One would thus rather expect a slight increase of the frequency of the Raman active mode with respect to the IR active mode¹⁶ and, accordingly, an increase of the frequency of the bulk Raman active mode with respect to the corresponding single-layer mode. As a plausible explanation of this anomalous trend the long range Coulomb interaction was mentioned.¹⁴ The purpose of our article is the clarification of this issue by a detailed *ab-initio* study of the inter-atomic force constants, separating the short-range and the long range Coulomb parts. We show in the following, that the anomalous trend in the E_{2g}^1 mode frequency is caused by the dielectric screening of the long range Coulomb forces in bulk MoS₂. At the same time, we present a full *ab-initio* study of the phonon dispersion relations of the phonon dispersion relations of single-layer and of bulk MoS₂ and the intimately related material WS₂. (Tungsten is in the same column of the periodic system as Molybdenum). Apart from a study of the vibrational stability of MoS₂ nanoribbons,¹⁷ a fully comprehensive *ab initio* study of the vibrational properties of these materials is still absent in the literature.

In Section II we present the methods for the calculation of the phonon dispersions and the analysis of the force constants. In section III we discuss the phonon dispersion relations of MoS₂ and WS₂ single layers and bulk and compare with experimental data. In section IV, we present the calculated results for the evolution of the Raman active phonon modes as a function of the number of

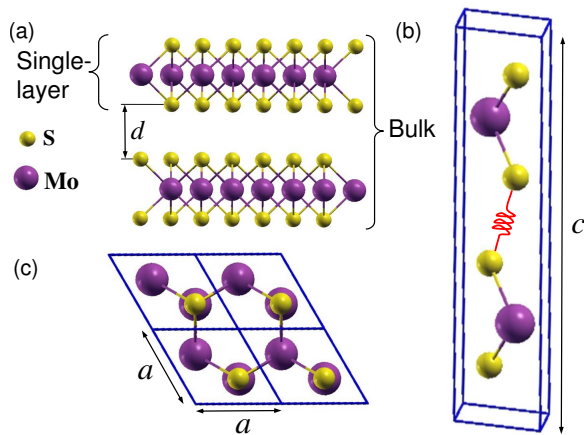


FIG. 1. (a) MoS₂ bulk and single-layer. The interlayer distance is denoted by d . (b) and (c) Side and top view of the MoS₂ bulk unit cell (analogously for WS₂) unit cell. The primitive vectors are $\mathbf{a} = (a, 0, 0)$, $\mathbf{b} = (a/2, \sqrt{3}a/2, 0)$, and $\mathbf{c} = (0, 0, c)$. The weak layer interaction is indicated by a spring.

layers and give an explanation in terms of the short-range and long-range contributions to the force constants.

II. CALCULATION METHODS

MoS₂ and WS₂ belong to the dichalcogenide family of materials, built up of weakly (van der Waals) bonded S-Mo-S single-layers as shown in Fig. 1. Each one of these single-layers consists of two hexagonal planes of S atoms and an intercalated hexagonal plane of Mo atoms bound with the sulfur atoms in a trigonal prismatic arrangement. The symmetry space group of bulk MoS₂ is $P3m1$ (point group D_{6h}). The space group of the single layer is $P6m2$ (point group D_{3h}). Consequently, systems with even number of layers belong to the space group $P3m1$ (with inversion symmetry), and systems with odd number of layers to the $P6m2$ space group (without inversion symmetry).

The phonon calculations begins with the determination of the equilibrium geometry (i.e. the relative atomic positions in the unit cell which yield zero forces and the lattice constants which leads to a zero-stress tensor). The calculations have been done with density functional theory (DFT) as implemented in the open-source code ABINIT,²⁰ within the local density approximation (LDA).²¹ We use Hartwigsen-Goedecker-Hutter pseudopotentials²² (including the semi-core electrons as valence electrons in the case of Mo and W) and a plane-wave cutoff at 60 Ha. The first Brillouin zone is sampled with a $12 \times 12 \times 4$ Monkhorst-Pack grid for bulk and $12 \times 12 \times 1$ for single and few-layers systems.

The optimized lattice parameters are shown in table I. The experimental lattice parameters of MoS₂ are $a = 3.15$ and $c = 12.3$ Å.¹⁸ In the case of WS₂ they are

$a = 3.153$ and $c = 12.323$ Å.²³ Our LDA calculations underestimate them by 0.7 % and 2.1 %, respectively. The slight underestimations of the in-plane lattice constant is a common feature of the LDA which tends to overestimate the strength of covalent bonds. For the single-layer, we checked the influence of the exchange-correlation potential on the geometry and the phonon dispersion by performing calculations within the Generalized Gradient Approximation (GGA).²⁴ For the single-layer of both MoS₂ and WS₂, we obtain a lattice constant $a = 3.18$ Å, 1.76 % larger than the LDA value and 0.96 % larger than the experimental (bulk) value. Correspondingly, the phonon frequencies are reduced by an almost constant factor of 1.04 % throughout the whole phonon dispersion.

The correct description of the c parameter is less evident because the LDA (and other semi-local functionals) completely neglect the van der Waals component of the inter-layer-interaction. At the same time, however, the LDA strongly overestimates the (weak) covalent part of the inter-layer bonding. Thus, the LDA has quite successfully reproduced the geometry and also given reasonable results for layer phonon modes of different layered materials such as graphite²⁵ and hexagonal boron nitride (hBN),²⁶ as well as of single-layers of hBN²⁷ and graphene²⁸ on a Ni(111) surface. We thus expect (and the obtained value for c supports this expectation) that the LDA works reasonably well for the inter-layer phonons of the MoS₂. We note that a physically correct description of the equilibrium geometry, and the potential energy surface around, would require the proper treatment of van der Waals contribution, e.g. on the level of the random-phase approximation as it has been done for bulk hBN²⁹ and for graphite.³⁰ Alternatively, non-local functionals that are optimized for the description of the van der Waals interaction³¹ could be used. Both approaches are, however, out of the scope of the present work.

For the calculations of single-layer and few-layers systems, we have used a periodic supercell, leaving enough distance between adjacent sheets. For instance, we use $c = 13.25$ Angstroms in the case of a single-layer. The remaining interlayer interaction has negligible effects on the phonon frequencies. All the results show a slight reduction of the in-plane lattice constant together with a slight stretching of the vertical distances, with the total effect of a smaller Mo-S bond length for decreasing number of layers, being 2.382 Å for single-layer and 2.384 Å for bulk MoS₂.

Once the equilibrium geometry has been obtained, the phonon frequencies ω can be calculated. These phonon frequencies are the solution of the secular equation

$$\left| \frac{1}{\sqrt{M_I M_J}} \tilde{C}_{I\alpha, J\beta}(\mathbf{q}) - \omega^2(\mathbf{q}) \right| = 0, \quad (1)$$

where \mathbf{q} is the phonon wave-vector, and M_I and M_J are the atomic masses of atoms I and J . The dynamical

| Lattice constants (Å) | | | |
|-----------------------|---------|---------|--------|
| MoS ₂ | 1-layer | 2-layer | Bulk |
| <i>a</i> | 3.125 | 3.126 | 3.127 |
| <i>c</i> | - | - | 12.066 |
| WS ₂ | 1-layer | 2-layer | Bulk |
| <i>a</i> | 3.125 | 3.125 | 3.126 |
| <i>c</i> | - | - | 12.145 |

TABLE I. Equilibrium lattice parameters of MoS₂ and WS₂ obtained in this work.

matrix is then defined as

$$\tilde{C}_{I\alpha,J\beta}(\mathbf{q}) = \frac{\partial^2 E}{\partial u_I^{\alpha*}(\mathbf{q}) \partial u_J^\beta(\mathbf{q})}, \quad (2)$$

where $u_I^\alpha(\mathbf{q})$ denotes the displacement of atom I in direction α . The second derivative of the energy in Eq. 2 corresponds to the change of the force acting on atom I in direction α with respect to a displacement of atom J in direction β .³⁴

$$\tilde{C}_{I\alpha,J\beta}(\mathbf{q}) = -\frac{\partial F_I^\alpha}{\partial u_J^\beta(\mathbf{q})}. \quad (3)$$

The Fourier transform of the \mathbf{q} -dependent matrix leads to the real space atomic force constant matrix $C_{I\alpha,J\beta}(\mathbf{R}_{IJ})$, where \mathbf{R}_{IJ} is the vector that joins atoms I and J . Thus, $C_{I\alpha,J\beta} < 0$ (> 0) means a binding (anti-binding) force in direction α acting on atom I when atom J is displaced in direction β . It is worth to mention that the diagonal term in the atom index, $C_{I\alpha,I\beta}$, corresponds, according to Newton's third law, to the total force exerted in the α -direction on the atom I , when the displacements of the atoms J in the β -direction is are set to one:³²

$$C_{I\alpha,I\beta}(\mathbf{0}) = \sum_{J \neq I}^{\infty} \frac{\partial F_I^\alpha}{\partial u_J^\beta}. \quad (4)$$

This term is always positive (unless the crystal is unstable) and in the following we refer to it as self-interaction. Eq. (4) demonstrates the contribution of many atoms to the self-interaction. One can distinguish two contributions, the short range part (which is mainly due to covalent bonding to the close neighbors) and the Ewald or long range part³³ (due to the Coulomb forces between the effective charges). This distinction will be helpful to interpret the evolution of the self interaction for varying layer thickness and to understand the unexpected trends of the phonon frequencies (section IV).

For the calculation of the dynamical matrix we have used density functional perturbation theory (DFPT)³⁴ where atomic displacements are taken as a perturbation

potential and the resulting changes in electron density and energy are calculated self-consistently through a system of Kohn-Sham like equations. Within this approach the phonon frequency can be obtained for arbitrary \mathbf{q} , with calculation only in a single unit-cell.

Since MoS₂ and WS₂ are slightly polar materials, certain IR active phonon modes at Γ give rise to a macroscopic electric field. This electric fields affects the longitudinal optical (LO) phonons in the limit $\mathbf{q} \rightarrow 0$, breaking the degeneracy of the LO mode with the transversal optical (TO) mode.³⁵ Thus, in bulk MoS₂ and WS₂, the nonanalytic part of the dynamical matrix (which contains the effective charges and the dielectric tensor) must be calculated in order to obtain the correct frequencies at the Brillouin zone-center.³⁶ The LO-TO splitting for the E_{1u} mode has the value of 2.8 cm⁻¹. In the case of a single or few-layers system, this effect is even smaller.

III. PHONON DISPERSIONS

A. MoS₂

We start our analysis of the vibrational properties with the description of the general features of the phonon dispersions of bulk and single-layer MoS₂, shown in Figure 2. We have also depicted the experimental data obtained with neutron inelastic scattering spectroscopy¹⁸. The overall agreement between theory and experiment is good, even for the inter-layer modes. This confirms our expectation that the LDA describes reasonably well the inter-layer interaction (even though not describing the proper physics of the inter-layer forces).

The bulk phonon dispersion has three acoustic modes. Those that vibrate in-plane (longitudinal acoustic, LA, and transverse acoustic, TA) have a linear dispersion and higher energy than the out-of-plane acoustic (ZA) mode. The latter displays a q^2 -dependence analogously to that of the ZA mode in graphene (which is a consequence of the point-group symmetry³⁷). The low frequency optical modes are found at 35.2 and 57.7 cm⁻¹ and correspond to rigid-layer shear/vertical motion, respectively (in analogy with the low frequency optical modes in graphite³⁸). When the wave number \mathbf{q} increases, the acoustic and low frequency optical branches almost match. It is worth to mention the absence of degeneracies at the high symmetry points M and K and the two crossings of the LA and TA branches just before and after the M point.

The high frequency optical modes are separated from the low frequency modes by a gap of 49 cm⁻¹. We have drawn in Fig. 3 the atomic displacements of the Raman active modes (E_{2g}^1 and A_{1g}) and the infrared active mode E_{1u} . The Raman active modes are also indicated in the phonon dispersion of Fig. 2. The in-plane modes E_{2g}^1 and E_{1u} are slightly split in energy (by 3 cm⁻¹). This is known as Davydov splitting and, for MoS₂, the experimental value is 1 cm⁻¹.¹⁵ However, the finding that the E_{1u} frequency is larger than that of the E_{2g}^1 mode con-

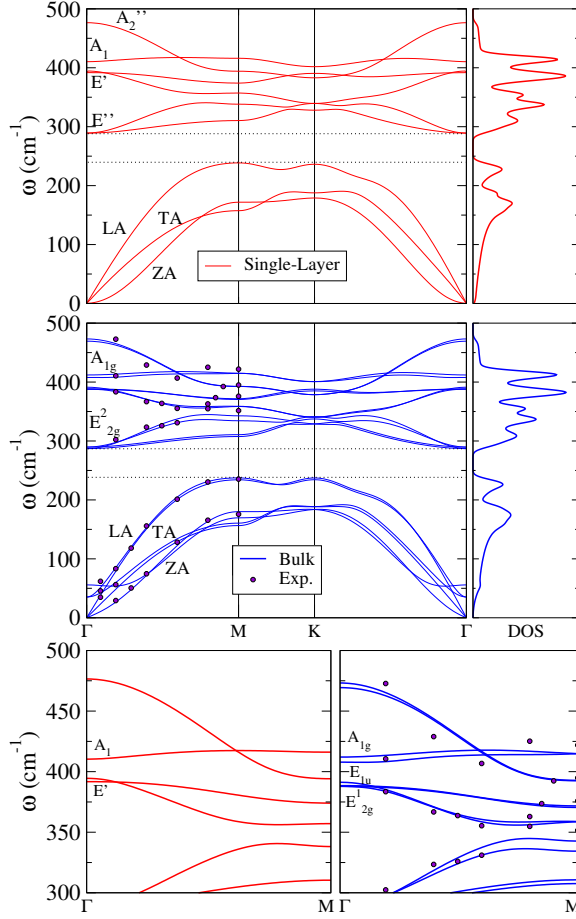


FIG. 2. Phonon dispersion curves and density of states of single-layer and bulk MoS₂. Points are experimental data extracted from Ref. 18. Low panel, inset of the phonon branches in the region of the E_{2g}^1 and A_{1g} modes.

tradicts *a priori* what one would expect from the weak inter-layer interaction: As one can see in Fig. 3, for the mode E_{2g}^1 , the sulfur atoms of different layers move in opposite direction and thus the additional “spring” between sulfur atoms of neighboring layers should increase the frequency of the mode E_{2g}^1 with respect of that of E_{1u} mode where sulfur atoms of neighboring sheets are moving in phase and thus the additional “spring” has no effect. The semi-empirical model of Ref. 16 takes this consideration into account, and obtained indeed that $\omega_{E_{2g}^1} > \omega_{E_{1u}}$ while experiments^{15,16} demonstrate the opposite behavior. Our *ab-initio* calculations match the experimental results which indicates that other causes beyond the weak inter-layer interaction are present in the system. We will analyze this feature in the next Section with the aid of the atomic force constants.

We now turn to analyze the single-layer phonon dispersion, shown in Fig. 2. The symmetry is reduced from D_{6h} to D_{3h} and there is no longer a center of inversion as in the bulk. Therefore, the phonon mode labels at Γ must

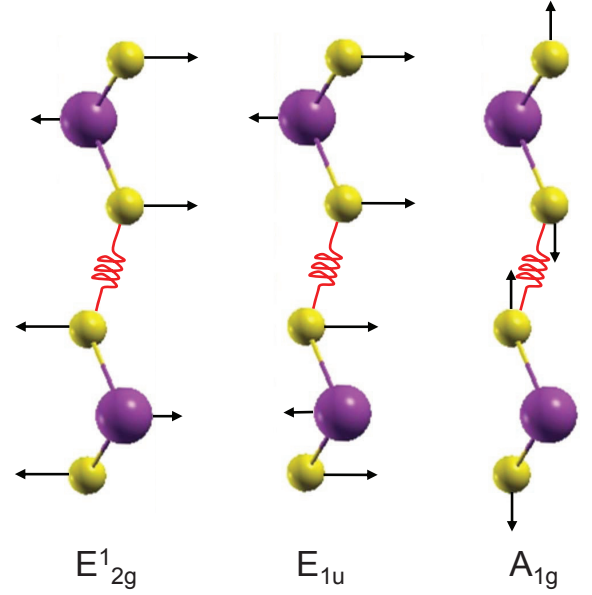


FIG. 3. Phonon modes in-plane E_{2g}^1 , E_{1u} , and the out-of-plane phonon mode A_{1g} , for the bulk MoS₂ (analogously for WS₂).

| D_{3h} | D_{6h} | Character | Direction | Atoms | ω_{MoS_2} (cm ⁻¹) | |
|----------|------------|--|--------------|-------|--------------------------------------|-------|
| A_2 | A_{2u} | Acoustic | Out-of-plane | Mo+S | 0.0 | 0.0 |
| | B_{2g}^2 | Inactive | Out-of-plane | Mo+S | - | 55.7 |
| - | E_{2g}^2 | Raman | In-plane | Mo+S | - | 35.2 |
| A_1 | A_{1g} | Raman | Out-of-plane | S | 410.3 | 412.0 |
| | B_{1u} | Inactive | Out-of-plane | S | - | 407.8 |
| A_2'' | A_{2u} | Infrared ($\mathbf{E} \mathbf{c}$) | Out-of-plane | Mo+S | 476.0 | 469.4 |
| | B_{2g}^1 | Inactive | Out-of-plane | Mo+S | - | 473.2 |
| E' | E_{2g}^1 | Raman | In-plane | Mo+S | 391.7 | 387.8 |
| | E_{1u} | Infrared ($\mathbf{E}\perp\mathbf{c}$) | In-plane | Mo+S | - | 391.2 |
| E'' | E_{1g} | Raman | In-plane | S | 289.2 | 288.7 |
| | E_{2u} | Inactive | In-plane | S | - | 287.1 |

TABLE II. Relevant phonon symmetry representations of single-layer (point group D_{3h}) and bulk (point group D_{6h}) MoS₂ (inspired in Table II of Ref. 15). Direction out-of-plane (in-plane) is parallel (perpendicular) to the \mathbf{c} vector of the unit cell, respectively. Phonon frequencies are the calculated values of this work.

be changed accordingly. The number of phonon branches is reduced to nine. Table II shows the most relevant MoS₂ single-layer and bulk modes at Γ , together with their character, displacement direction, involved atoms, and frequency.

Overall, the single-layer and bulk phonon dispersions have a remarkable resemblance. In the bulk, all single-layer modes are split into two branches but since the inter-layer interaction is weak, the splitting is very low (similar to the situation in graphite and graphene.³⁸ The

only notable exception from this is the splitting of the acoustic modes around Γ . In the single-layer, the resulting low frequency optical modes are absent.

In the single layer, the high frequency Γ modes E_{2g}^1 and E_{1u} collapse into the mode E' . (From Fig. 3 it is evident that with increasing inter-layer distance, the modes E_{2g}^1 and E_{1u} acquire the same frequency.) Interestingly, as measured in Ref. 14 and indicated in Table II, the bulk E_{2g} mode is lower in frequency than the single-layer E' mode. This contradicts the expectation that the additional inter-layer interaction should increase the frequency but is in line with the anomalous sign of the Davydov splitting between the bulk E_{2g}^1 and E_{1u} modes. The origin of this will be discussed in section IV. The out-of-plane mode A_{1g} follows the expected trend that the inter-layer interaction increases the frequency with respect to the single-layer mode A_1 .

The densities of states (DOS) of single-layer and bulk are represented in the right panels of Fig. 3. The differences between single-layer and bulk DOS are minimal, except a little shoulder around 60 cm^{-1} in the bulk DOS due to the low frequency optical modes. In both cases the highest peaks are located close to the Raman active modes E_{2g}^1 and A_{1g} .

B. WS_2

Figure 4 shows the phonon dispersions of single-layer and bulk WS_2 , together with the density of states (DOS). The general features are identical to those of the dispersions of MoS_2 (Fig. 2). The differences between single-layer and bulk dispersions are similarly weak as in the case of MoS_2 . Thus, also the bulk DOS resembles very much that of the single-layer (except for the small shoulder $\sim 50 \text{ cm}^{-1}$ due to the inter-layer optical modes).

For a better comparison of MoS_2 and WS_2 single-layer phonon frequencies, we have depicted them together in Fig. 5. In general, the WS_2 phonon bands are shifted down to lower frequencies with respect to the MoS_2 frequencies. The cause of this trend is the larger mass of the tungsten atoms, and therefore their lower vibration frequency (see Eq. 1). The only notable exceptions from this general downshift are the branches associated to the mode E'' , around 300 cm^{-1} and to the A_1 mode around 410 cm^{-1} . In these modes, only the sulfur atoms are vibrating (see Table II) and thus their frequency is not affected by the mass of the metal atom (W or Mo), just by the strength of the covalent bond.

The larger mass of W leads to a larger frequency gap between low and high frequency modes (110 cm^{-1}) since the highest acoustic branch is pushed down. Furthermore, the difference between the modes A_1 and E' , is now of 60 cm^{-1} , three times larger than in the case of MoS_2 .

The density of states of the WS_2 single-layer is also appreciably different from that of MoS_2 . While at low frequencies the DOS has two well differentiated peaks, as

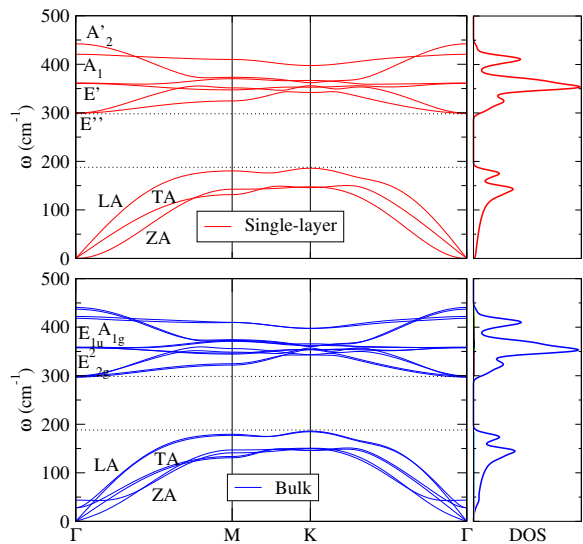


FIG. 4. Phonon dispersion curves and density of states of 1-layer and bulk WS_2 .

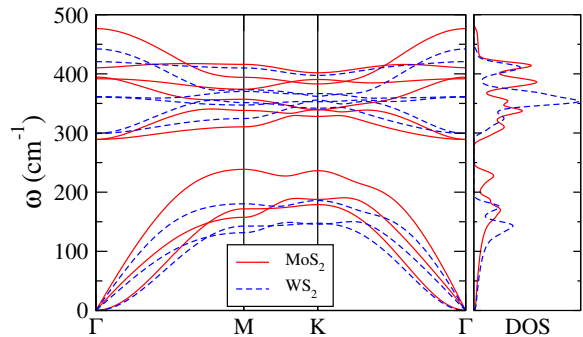


FIG. 5. Phonon dispersion curves for single-layer of MoS_2 (solid lines) and WS_2 (dashed lines). The density of states is depicted in the right panel.

in Fig. 2, for higher energies one peak stands out from the others, at frequency of $\sim 350 \text{ cm}^{-1}$, and associated mainly to the Γ -point mode E' .

IV. EVOLUTION OF A_{1g} AND E_{2g}^1 PHONON MODES WITH THE NUMBER OF LAYERS

The understanding of the frequency trends of the A_{1g} and E_{2g} modes with varying layer thickness requires a more refined analysis. With the aim of explaining the Raman scattering experiments of Ref. 14 we have calculated the phonon frequencies at the Γ point for single, double- and triple-layers and we discuss the evolution of the atomic force constants from single-layer to bulk in detail.

Figure 6 shows the phonon frequency of A_{1g} and E_{2g}^1 modes as a function of the number of layers. Since LDA

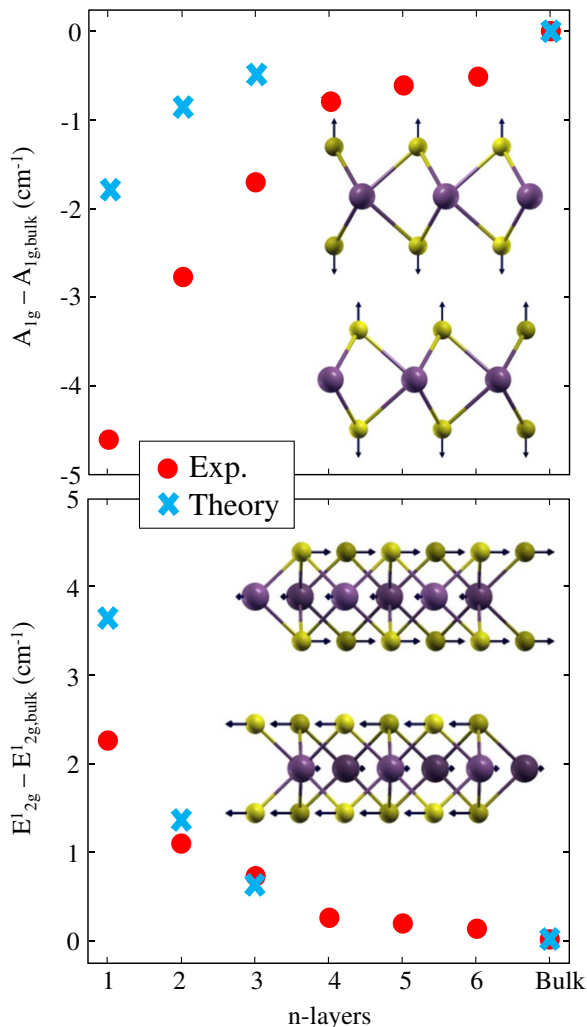


FIG. 6. Phonon frequencies of A_{1g} and E_{2g}^1 modes as a function of MoS₂ layer thickness, as obtained in this work (squares) and experimental data from Ref. 14 (circles). We plot the frequency differences with respect to the corresponding bulk modes. The insets represent the phonon modes at Γ point.

tends to overestimate the phonon frequencies, it is reasonable to represent the difference between the n -layers frequency and the bulk frequency instead of comparing absolute theoretical and experimental values. In such a representation we observe that our calculation properly reproduce the up-shift of the A_{1g} mode and the down-shift of the E_{2g}^1 mode with increasing layer number. The quantitative differences between theory and experiment are mainly due to the limited precision of the description of the inter-layer interaction by the LDA.

After we have shown that DFPT-LDA reproduces the experimental trends we would like to give an explanation of this behavior, taking advantage of the detailed knowledge of the atomic force constants, available in *ab initio* methods. We interpret the changes in phonon fre-

quency through an analysis of the real-space force constants (Eq. 3), in particular of the self-interaction term (Eq. 4). Going from the single-layer to a multi-layer, this term changes in two ways: i) the short range term increases due to the (weak, but non-negligible) interaction with atoms from neighboring layers; (ii) the long-range Coulomb interaction changes, because the sum extends over effective charges from all layers and the effective screening of the Coulomb potential increases.

We start our analysis with the out-of-plane mode A_{1g} . From Fig. 3, it is intuitively clear that the interaction between sulfur atoms of neighboring layers can influence substantially the frequency. Going from the single-layer to the double-layer, one “adds” an additional “spring” between the atoms S and S’ on neighboring layers which leads to an increase of the A_{1g} mode frequency with increasing number of layers. As only sulfur atoms are involved in this mode, we just need to examine the sulfur self-interaction term (C_{S_z, S_z}) and the atomic force constant (C_{S_z, S'_z}) between nearest neighbors, that belong to adjacent layers (atoms joined by the spring in Fig. 3). We have summarized in Table III the results. Note that the small variation of the term C_{S_z, S_z} from single-layer to bulk prevents it from being the main cause of a frequency increasing of almost 5 cm⁻¹. Thus, the term C_{S_z, S'_z} has a negative value which implies a binding force (“spring”) between atoms S and S’ which leads to an increase of frequency. Force constants related to farer neighbors are negligible in comparison with C_{S_z, S'_z} . This demonstrates that the weak interlayer interaction is the main cause of the frequency increasing with the number of layers.

One might expect that the same argument holds for the E_{2g}^1 mode: the additional “spring” between sulfur atoms from neighboring layers should increase the frequency with increasing number of layers as well. However, theoretical and experimental results show the opposite behavior. The reason can be found in the self-interaction terms $C_{Mox, Mox}$ for Mo and S in Table 3: while the difference between single-layer and bulk is negligible for the sulfur atoms, one observes a considerable decrease for the molybdenum atoms. Interestingly, the short range contribution to the self-interaction increases (as one would expect from the inter-layer interaction). However, the long-range Coulomb part³³ decreases considerably. In the appendix, we show that this decrease is related to the strong increase of the dielectric tensor (both in-plane and out-of-plane) when going from the single-layer (represented in our calculations by a periodic stacking of single-layers with large vacuum between) to the bulk (see Table III). We note that one might associate the change in frequency to the differences in lattice constant and interatomic distances in bulk and single-layer, respectively. However, the small differences shown in Section II are not enough to account for the observed magnitude of the E_{2g}^1 frequency change.³⁹

Therefore, the decrease of the E_{2g}^1 phonon frequency is associated to a stronger dielectric screening of the long range Coulomb interaction in few-layer and bulk MoS₂.

The effect is particularly pronounced for the molybdenum atoms, as Table III shows. Our analysis also explains why previous empirical models have not been able to explain the experimental observations, due to the difficulty to include this subtle change in the parameters.

V. CONCLUSIONS

In conclusion, we have studied the phonon dispersions of MoS₂ and WS₂ single layers and bulk using density functional perturbation theory in the local density approximation. We obtain good agreement with neutron diffraction data as well as Raman and infrared absorption spectroscopies. We have explored how the Raman active modes A_{1g} and E_{2g}^1 change their frequencies when the number of layers varies, and confirm the recently reported down-shift of the E_{2g}^1 mode with increasing number of layers. This unexpected behavior can be explained by an increase of the dielectric screening which reduces the long range Coulomb interaction between the effective charges and thus reduces the overall restoring force on the atoms. We expect that this explanation also holds for other polar layered materials where an anomalous Davydov splitting has been observed (such as GaSe⁴⁰ and GaS⁴¹) or where the Raman peak shifts down with increasing number of layers such as it has been recently observed for hexagonal BN.⁴²

ACKNOWLEDGMENTS

Funding was provided by the French National Research Agency (ANR) through project bl-inter09_482166. Calculations were done at the IDRIS supercomputing center, Orsay (Proj. No. 091827).

Appendix A

The examination of the long-range atomic force constant formula can help to establish quantitatively its change with the variation of the dielectric tensor in the single-layer and bulk MoS₂. However, the anisotropy of the crystalline structure of MoS₂ impedes a direct relation between the long range atomic force constants

and the dielectric tensor. The long range contribution, $C_{I\alpha,J\beta}^{lr}$, can be written in terms of the dielectric tensor ϵ , its inverse, ϵ^{-1} , the Born effective charges $Z_{I,\alpha\alpha'}^*$, and the interatomic distance $\mathbf{d} \equiv \mathbf{d}_{IJ}$, as defined in Ref. 33:

$$C_{I\alpha,J\beta}^{lr} = \sum_{\alpha',\beta'} Z_{I,\alpha,\alpha'}^* Z_{J,\beta,\beta'}^* \left(\frac{(\epsilon^{-1})_{\alpha'\beta'}}{D^3} - 3 \frac{\Delta_{\alpha'} \Delta_{\beta'}}{D^5} \right) \times (\det \epsilon)^{-1/2},$$

where $\Delta_\alpha = \sum_\beta (\epsilon^{-1})_{\alpha\beta} d_\beta$ is the conjugate of the vector \mathbf{d} , and the norm of the latter in this metrics is $D = \sqrt{\Delta \cdot \mathbf{d}}$. This expression simplifies enormously by assuming diagonal the dielectric tensor, and $Z_{I,\alpha\alpha'}^* \equiv Z_{I,\alpha\alpha'}^* \delta_{\alpha\alpha'}$. After some algebra one obtains:

$$C_{I\alpha,J\beta}^{lr} = \frac{Z_{I,\alpha\alpha}^* Z_{J,\beta\beta}^*}{\sqrt{\epsilon_{xx}\epsilon_{yy}\epsilon_{zz}}} \left(\frac{\epsilon_{\alpha\beta}^{-1} \delta_{\alpha\beta}}{D^3} - 3 \frac{\epsilon_{\alpha\alpha}^{-1} \epsilon_{\beta\beta}^{-1} d_\alpha d_\beta}{D^5} \right). \quad (\text{A1})$$

We can examine with an example how the long-range atomic force constants of single-layer and bulk MoS₂ are related with the dielectric tensors. Thus, we can evaluate the term $C_{I\alpha,J\beta}^{lr}$ for neighbor Mo atoms that belong to the same layer, with interatomic distance $\mathbf{d} = (d, 0, 0)$, and assuming the same distance for single-layer and bulk. Thus, we obtain a simplified expression of Eq. A1:

$$C_{Mo,x,Mo,x}^{lr} = -2 \frac{(Z_{Mo,x,x}^*)^2}{\sqrt{\epsilon_{xx}\epsilon_{zz}} d^3}. \quad (\text{A2})$$

The Born effective charges $Z_{Mo,x,x}^*$ are almost equal for both systems, and using the dielectric tensors given in Table III, we obtain:

$$\frac{C_{Mo,x,Mo,x}^{lr}(1l)}{C_{Mo,x,Mo,x}^{lr}(bulk)} = \sqrt{\frac{\epsilon_{xx,bulk}\epsilon_{zz,bulk}}{\epsilon_{xx,1l}\epsilon_{zz,1l}}} = 3.09. \quad (\text{A3})$$

From the *ab-initio* calculation of the atomic constants we obtain $C_{Mo,x,Mo,x}^{lr}(1l)/C_{Mo,x,Mo,x}^{lr}(bulk) = 3.19$, which is in agreement with the value obtained in Eq. A3. This demonstrates that the difference in the long-range part of the force constants for single-layer and bulk originates from the different dielectric screening.

* corresponding author: alejandro.molina@isen.iemn.univ-lille1.fr

¹ K. S. Novoselov, D. Jiang, F. Schedin, T. J. Booth, V. V. Khotkevich, S. V. Morozov, and A. K. Geim. Proc. Natl. Acad. Sci. U.S.A. **102**, 10451 (2005).

² K. S. Novoselov, A. K. Geim, S. V. Morozov, D. Jiang, Y. Zhang, S. V. Dubonos, I. V. Grigorieva, A. A. Firsov. Science **306**, 666 (2004).

³ P. R. Wallace. Phys. Rev. **71**, 622 (1947).

⁴ A. K. Geim and K. S. Novoselov. Nat Mater **6**, 183 (2007).

⁵ Y.-W. Son, M.L. Cohen, and S.G. Louie, Phys. Rev. Lett. **97**, 216803 (2006).

⁶ G. Giovannetti, P.A. Khomyakov, G. Brocks, P.J. Kelly, and J. van den Brink, Phys. Rev. B **76**, 073103 (2007)

⁷ Y. Zhang, T.-T. Tang, C. Girit, Z. Hao, M. C. Martin, A. Zettl, M. F. Crommie, Y. R. Shen, and F. Wang. Nature

| Atom | | C_{S_z, S_z} | C_{S_z, S'_z} | $C_{M_{ox}, M_{ox}}$ | Long-range | Short-range | $\epsilon_{xx} = \epsilon_{yy}$ | ϵ_{zz} |
|---------|----|----------------|-----------------|----------------------|------------|-------------|---------------------------------|-----------------|
| Bulk | Mo | - | - | 0.27660 | 0.00308 | 0.27352 | 15.40 | 7.43 |
| | S | 0.15837 | -0.00099 | 0.12310 | 0.00071 | 0.12239 | | |
| 1-layer | Mo | - | - | 0.28275 | 0.01058 | 0.27217 | 7.36 | 1.63 |
| | S | 0.15860 | - | 0.12320 | 0.00265 | 0.12055 | | |

TABLE III. Self-interaction term C_{S_α, S_α} and $C_{M_{\alpha\alpha}, M_{\alpha\alpha}}$ of the Mo and S atoms, and atomic force constants between S atoms of adjacent layers, C_{S_z, S'_z} , as defined in Section II (atomic units). The dielectric tensor ϵ of both systems is also given (non-diagonal elements are zero).

- 459, 820 (2009).
- ⁸ M. Y. Han, B. Ozyilmaz, Y. Zhang and P. Kim, Phys. Rev. Lett. **98**, 206805 (2007).
- ⁹ A. Splendiani, L. Sun, Y. Zhang, T. Li, J. Kim, C.-Y. Chim, G. Galli, and F. Wang. Nano Lett. **10**, 1271 (2010).
- ¹⁰ K. F. Mak, C. Lee, J. Hone, J. Shan, and T. F. Heinz. Phys. Rev. Lett. **105**, 136805 (2010).
- ¹¹ B. Radisavljevic, A. Radenovic, J. Brivio, V. Giacometti, and A. Kis. Nat Nano **6**, 147 (2011).
- ¹² J. N. Coleman, M. Lotya, A. O'Neill, S. D. Bergin, P. J. King, U. Khan, K. Young, A. Gaucher, S. De, R. J. Smith, I. V. Shvets, S. K. Arora, G. Stanton, H.-Y. Kim, K. Lee, G. T. Kim, G. S. Duesberg, T. Hallam, J. J. Boland, J. J. Wang, J. F. Donegan, J. C. Grunlan, G. Moriarty, A. Shmeliov, R. J. Nicholls, J. M. Perkins, E. M. Grievson, K. Theuwissen, D. W. McComb, P. D. Nellist, and V. Nicolosi. Science **331**, 568 (2011).
- ¹³ O. L. Krivanek, M. F. Chisholm, V. Nicolosi, T. J. Pennycook, G. J. Corbin, N. Dellby, M. F. Murfitt, C. S. Own, Z. S. Szilagyi, M. P. Oxley, S. T. Pantelides, and S. J. Pennycook. Nature **464**, 571 (2010).
- ¹⁴ C. Lee, H. Yan, L. E. Brus, T. F. Heinz, J. Hone, and S. Ryu. ACS Nano **4**, 2695 (2010).
- ¹⁵ T. J. Wieting and J. L. Verble. Phys. Rev. B **3**, 4286 (1971).
- ¹⁶ P. N. Ghosh and C. R. Maiti. Phys. Rev. B **28**, 2237 (1983).
- ¹⁷ C. Ataca, H. Sahin, E. Aktürk, and S. Ciraci, J. Phys. Chem. C **115**, 3934 (2011).
- ¹⁸ N. Wakabayashi, H. G. Smith, and R. M. Nicklow. Phys. Rev. B **12**, 659 (1975).
- ¹⁹ T. Livneh and E. Sterer. Phys. Rev. B **81**, 195209 (2010).
- ²⁰ X. Gonze, J.-M. Beuken, R. Caracas, F. Detraux, M. Fuchs, G.-M. Rignanese, L. Sindic, M. Verstraete, G. Zerah, F. Jollet, M. Torrent, A. Roy, M. Mikami, Ph. Ghosez, J.-Y. Raty, D.C. Allan, Comp. Mat. Sci. **25**, 478 (2002). The ABINIT code results from a common project of the Université Catholique de Louvain, Corning Incorporated, and other collaborators (<http://www.abinit.org>).
- ²¹ W. Kohn and L. J. Sham. Phys. Rev. **140**, A1133 (1965).
- ²² C. Hartwigsen, S. Goedecker, J. Hutter, Phys. Rev. B **58**, 3641 (1998).
- ²³ W. J. Schutte, J. L. de Boer, and F. Jellinek, J. Solid State Chem. **70**, 207 (1987).
- ²⁴ J. P. Perdew, K. Burke, and M. Ernzerhof, Phys. Rev. Lett. **77**, 3865 (1996).
- ²⁵ G. Kresse, J. Furthmüller, and J. Hafner, Europhys. Lett. **32**, 729 (1995).
- ²⁶ G. Kern, G. Kresse, and J. Hafner, Phys. Rev. B **59**, 8551 (1999).
- ²⁷ J. Serrano, A. Bosak, R. Arenal, M. Krisch, K. Watanabe, T. Taniguchi, H. Kanda, A. Rubio, and L. Wirtz, Phys. Rev. Lett. **98**, 095503 (2007).
- ²⁸ A. Allard and L. Wirtz, Nano Lett. **10**, 4335 (2010).
- ²⁹ A. Marini, P. Garcia-Gonzalez, A. Rubio, Phys. Rev. Lett. **96** 136404 (2006).
- ³⁰ S. Lebègue, J. Harl, Tim Gould, J. G. Angyán, G. Kresse, and J. F. Dobson, Phys. Rev. Lett. **105**, 196401 (2010).
- ³¹ H. Rydberg, M. Dion, N. Jacobson, E. Schröder, P. Hyldgaard, S. I. Simak, D. C. Langreth, and B. I. Lundqvist. Phys. Rev. Lett. **91**, 126402 (2003).
- ³² P. Brüesch. *Phonons: Theory and Experiments I* (Springer-Verlag, 1982).
- ³³ X. Gonze and C. Lee. Phys. Rev. B **55**, 10355 (1997).
- ³⁴ S. Baroni, S. de Gironcoli, A. Dal Corso, and P. Giannozzi. Rev. Mod. Phys. **73**, 515 (2001).
- ³⁵ M. Cardona and P. Y. Yu. *Fundamentals of Semiconductors* (Springer-Verlag, 1996).
- ³⁶ P. Giannozzi, S. de Gironcoli, P. Pavone, and S. Baroni. Phys. Rev. B **43**, 7231 (1991).
- ³⁷ R. Saito, G. Dresselhaus, and M. S. Dresselhaus. *Physical Properties of Carbon Nanotubes* (Imperial College Press, London, 1998).
- ³⁸ L. Wirtz and A. Rubio. Solid State Commun. **131**, 141 (2004).
- ³⁹ In order to proof this hypothesis, we have also examined the frequencies of a single-layer setting bulk interatomic distances, in order to mimic as much as possible the bulk environment onto the single layer. The E_{2g}^1 is now 390.3 cm^{-1} , which is still larger than the bulk, with a value of 387.8 cm^{-1} . Therefore, we can neglect the distinct interatomic distances as the main cause of the E_{2g}^1 frequency trend.
- ⁴⁰ T.J. Wieting and J.L. Verble, Phys. Rev. B **5**, 1473 (1972).
- ⁴¹ N. Kuroda and Y. Nishina, Phys. Rev. B **19**, 1312 (1979).
- ⁴² R.V. Gorbachev, I. Riaz, R.R. Nair, R. Jalil, L. Britnell, B.D. Belle, E.W. Hill, K.S. Novoselov, K. Watanabe, T. Taniguchi, A.K. Geim, and P. Blake, Small **7**, 465 (2011).